

## PAPER

## Wave Scattering from an Apodised Sinusoidal Surface

Junichi NAKAYAMA<sup>†a)</sup>, *Regular Member*

**SUMMARY** This paper deals with the scattering of a TE plane wave by an apodised sinusoidal surface. The analysis starts with the extended Floquet solution, which is a ‘Fourier series’ with ‘Fourier coefficients’ given by band-limited Fourier integrals of amplitude functions. An integral equation for the amplitude functions is derived and solved by the small perturbation method to get single and double scattering amplitudes. Then, it is found that the beam shape generated by the single scattering is proportional to the Fourier spectrum of the apodisation function, but that generated by the double scattering is proportional to the spectrum of the squared apodisation. As a result, the single scattering beam and the double scattering beam may have different sidelobe patterns. It is demonstrated that the sidelobes are much reduced if Hanning window or Hamming window is used as an apodisation function.

**key words:** *periodic Fourier transform, wave scattering, finite periodic surface*

## 1. Introduction

This paper deals with the scattering of a TE plane wave from an apodised sinusoidal surface shown in Fig. 1.

The wave scattering by a periodically corrugated surface with finite extent has received much interest, because it is related with important applications [1]–[6] such as diffraction gratings, leaky wave antenna and waveguide couplers in thin film optics. Physically speaking, the wave scattered from a finite periodic surface is made up of several beams, which are diffracted into the directions determined by the famous grating formula [7]. Due to the interferences between waves radiated from the ends of the corrugation, sidelobes appears as ripples in the angular distribution of the scattering [2]–[4], [8]. This paper proposes an apodised periodic corrugation to reduce the sidelobe levels. We will demonstrate that the sidelobes are much reduced in level and in angular distribution if Hanning window or Hamming window [9] is used as an apodisation function.

For analysis, we employ the method of periodic Fourier transform introduced in a previous paper [8], where the scattered wave was shown to have an extended Floquet solution in case of a periodic corrugated surface with finite extent. The extended Floquet solution is a ‘Fourier series’ with ‘Fourier coefficients’

given by band-limited Fourier integrals of amplitude functions. From the boundary condition, we obtain an integral equation for the amplitude functions. Assuming the corrugation amplitude is sufficiently small, we solve the integral equation by the small perturbation method. We obtain the first and second order solutions, which represent the single and double scattering processes, respectively. Then, it is found that the beam shape generated by the single scattering is proportional to the Fourier spectrum of the apodisation function, but that generated by the double scattering is proportional to the spectrum of the squared apodisation. We conclude that the single scattering beam and the double scattering beam may have different sidelobe patterns.

Properties of the periodic Fourier transform are summarized in Appendix.

## 2. Formulation

Let us consider the wave scattering from a periodically corrugated plane shown in Fig. 1. We write the surface deformation as

$$z = f(x) = \sigma g(x|W) \sin(k_L x), \quad k_L = \frac{2\pi}{L}, \quad (1)$$

where  $L$  is the period,  $\sigma$  is the corrugation height parameter,  $W$  is the physical length of corrugation and  $g(x|W)$  is the apodisation factor which is a non-negative function taking its maximum at  $x = 0$ ,

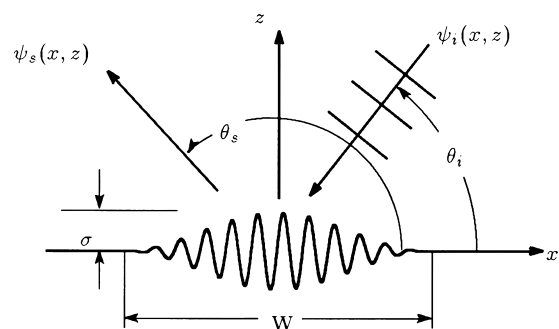


**Fig. 1** Scattering and diffraction of a plane wave from a periodically corrugated surface with apodisation. The incident plane wave and the scattered wave are denoted by  $\psi_i(x, z)$  and  $\psi_s(x, z)$ , respectively.  $\theta_i$  is the angle of incidence and  $\theta_s$  is a scattering angle.  $W$  is the physical length of corrugation and  $\sigma$  is the corrugation height parameter.

Manuscript received December 8, 1999.

<sup>†</sup>The author is with the Faculty of Engineering and Design, Kyoto Institute of Technology, Kyoto-shi, 606-8585 Japan.

a) E-mail: nakayama@dj.kit.ac.jp

$$g(0|W) = \max_x [g(x|W)] = 1, \tag{2}$$

and vanishes for  $|x| > W/2$ ,

$$g(x|W) = 0, \quad |x| > \frac{W}{2}. \tag{3}$$

We denote the  $y$  component of the electric field by  $\psi(x, z)$ , which satisfies the wave equation

$$\left[ \frac{\partial^2}{\partial x^2} + \frac{\partial^2}{\partial z^2} + k^2 \right] \psi(x, z) = 0, \tag{4}$$

in the region  $z > f(x)$  and the Dirichlet condition

$$\psi(x, z) = 0, \quad z = f(x), \tag{5}$$

on the surface. Here,  $k = 2\pi/\lambda$  is the wave number and  $\lambda$  is the wavelength.

We write the incident plane wave  $\psi_i(x, z)$  as

$$\psi_i(x, z) = e^{-ipx} e^{-i\beta_0(p)z}, \quad p = k \cdot \cos \theta_i, \tag{6}$$

$$\beta_m(p) = \sqrt{k^2 - (p + mk_L)^2}, \quad \text{Im}[\beta_m(p)] \geq 0, \tag{7}$$

$$(m = 0, \pm 1, \pm 2, \dots),$$

where  $\theta_i$  is the angle of incidence. Since the surface becomes flat for  $|x| > W/2$ , we put the electric field as

$$\psi(x, z) = e^{-ipx} e^{-i\beta_0(p)z} - e^{-ipx} e^{i\beta_0(p)z} + \psi_s(x, z), \tag{8}$$

where  $e^{-ipx} e^{i\beta_0(p)z}$  is the specularly reflected wave and  $\psi_s(x, z)$  is the scattered wave due to surface deformation.

In view of the periodic nature of the surface corrugation, we may determine a possible form of the scattered wave. By use of the periodic Fourier transform and its inverse transformation, it was shown in a previous paper [8] that the scattered wave may have an extended Floquet form:

$$\psi_s(x, z) = \frac{1}{k_L} \sum_{m=-\infty}^{\infty} e^{-imk_L x} \times \int_{-\pi/L}^{\pi/L} A_m(s) e^{-i(p+s)x + i\beta_m(p+s)z} ds, \tag{9}$$

which satisfies the wave Eq. (4) and radiation condition for  $z \rightarrow \infty$ . Here,  $A_m(s)$  is the complex amplitude of the plane wave propagating with wave vector  $\mathbf{k} = -(s + p + mk_L)\mathbf{e}_x + \beta_m(p+s)\mathbf{e}_z$ ,  $\mathbf{e}_x$  and  $\mathbf{e}_z$  being unit vectors in the  $x$  and  $z$  directions, respectively. In other words,  $A_m(s)$  is the amplitude of the plane wave scattered into the direction  $\theta_s$  determined by,

$$\cos \theta_s = - \left( \cos \theta_i + \frac{s}{k} + m \frac{\lambda}{L} \right). \tag{10}$$

If we put  $s = 0$ , (10) is reduced to the famous grating formula:

$$\cos \theta_m = - \left( \cos \theta_i + m \frac{\lambda}{L} \right), \tag{11}$$

where  $\theta_m$  is the  $m$ th order diffraction angle. Equation (9) is a ‘Fourier series’ with ‘Fourier coefficients’ given by band-limited Fourier integrals of amplitude functions  $A_m(s)$ .

The diffracted waves are physically radiated from the corrugated part of the surface. Therefore, the diffracted waves exist only limited regions in space and in the far region they become beams propagating into  $\theta_s = \theta_m$  given by (11). In the angular distribution of the scattering, such a beam appears as a mainlobe at  $\theta_s = \theta_m$  with a finite beam width. The amplitude of each beam is physically expected to be proportional to  $W$  the width of corrugation. To represent the effects of apodisation precisely, however, we introduce the width parameter  $W_n$  and the spectrum function  $G_n(s|W)$  as

$$G_n(s|W) = \int_{-\infty}^{\infty} e^{isx} [g(x|W)]^n dx, \tag{12}$$

$$W_n = G_n(0|W) \geq |G_n(s|W)|, \quad (n = 1, 2, \dots), \tag{13}$$

where the inequality holds because  $g(x|W)$  is non-negative. By the Parseval relation and (13), we obtain

$$\frac{1}{2\pi} \int_{-\infty}^{\infty} |G_n(s|W)|^2 ds = \int_{-\infty}^{\infty} |g(x|W)|^{2n} dx = W_{2n} \tag{14}$$

Then, we define the spectrum width  $\Delta S^{(n)}$

$$\Delta S^{(n)} = \frac{\int_{-\infty}^{\infty} |G_n(s|W)|^2 ds}{|G_n(0|W)|^2} = 2\pi \frac{W_{2n}}{W_n^2}, \quad (n = 1, 2, \dots), \tag{15}$$

which is the half-power width shown in Fig. 2.

Applying the saddle point method to (9), we obtain the scattered wave in the far field, from which the scattering cross section  $\sigma(\theta_s|\theta_i)$  is derived as

$$\begin{aligned} \sigma(\theta_s|\theta_i) &= \lim_{r \rightarrow \infty} 2\pi \frac{kr}{kW_1} \cdot |\psi_s(r \cos \theta_s, r \sin \theta_s)|^2 \\ &= \sum_{m=-\infty}^{\infty} \frac{(2\pi k)^2}{k_L^2 kW_1} |A_m(-k \cos \theta_s - p - mk_L)|^2 \end{aligned}$$

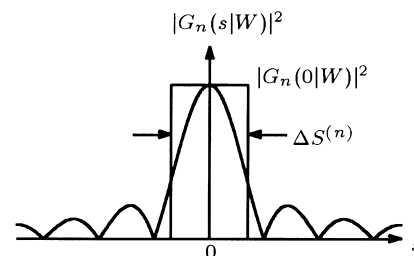


**Fig. 2** Power spectrum  $|G_n(s|W)|^2$  and spectrum width  $\Delta S^{(n)}$ . Since  $g(x|W)$  is a non-negative function of  $x$ ,  $|G_n(s|W)|^2$  becomes maximum at  $s = 0$ .

$$\times \sin^2 \theta_s u(-k \cos \theta_s - p - mk_L |k_L), \quad (16)$$

where  $\theta_s$  and  $\theta_i$  are a scattering angle and the angle of incidence, respectively (See Fig. 1). Here,  $u(s|k_L)$  is a rectangular function

$$u(s|k_L) = u^2(s|k_L) = \begin{cases} 1, & |s| \leq k_L/2 \\ 0, & |s| > k_L/2 \end{cases}. \quad (17)$$

We note that  $\sigma(\theta_s|\theta_i)$  is a non-dimensional quantity because it is divided by the width parameter  $W_1$ .

### 3. Integral Equation

In this section, we will obtain an integral equation for the amplitude  $A_m(s)$ . By the Rayleigh hypothesis, we assume the expansion (9) is valid even on the corrugated part of the surface. Substituting (8) and (9) into the boundary condition (5), we obtain

$$\begin{aligned} \frac{1}{k_L} \sum_{m=-\infty}^{\infty} e^{-imk_L x} \int_{-\pi/L}^{\pi/L} A_m(s) e^{-is'x + i\beta_m(p+s')f(x)} ds' \\ = -[e^{-i\beta_0(p)f(x)} - e^{i\beta_0(p)f(x)}]. \end{aligned} \quad (18)$$

We decompose the exponential factor in (18) as

$$e^{i\beta_m(p+s')f(x)} = 1 + f_e[x, \sigma\beta_m(p+s')], \quad (19)$$

where the first term 1 in the right-hand side implies the flat surface ( $z = f(x) \equiv 0$ ). The second term is the effect of variation from the flat surface,

$$\begin{aligned} f_e[x, \sigma\beta_m(p+s')] \\ = \exp[i\sigma\beta_m(p+s')g(x|W) \sin(k_L x)] - 1 \end{aligned} \quad (20)$$

which vanishes when  $|x| > W/2$  by (3). By the decomposition, (18) becomes

$$\begin{aligned} \frac{1}{k_L} \sum_{m=-\infty}^{\infty} e^{-imk_L x} \int_{-\pi/L}^{\pi/L} A_m(s') e^{-is'x} ds' \\ + \frac{1}{k_L} \sum_{m=-\infty}^{\infty} e^{-imk_L x} \int_{-\pi/L}^{\pi/L} A_m(s') e^{-is'x} f_e[x, \\ \sigma\beta_m(p+s')] ds' = f_e[x, \sigma\beta_0(p)] - f_e[x, -\sigma\beta_0(p)]. \end{aligned} \quad (21)$$

Using (A.4) and (A.6), we next calculate the periodic Fourier transform of (21) to obtain,

$$\begin{aligned} \sum_{m=-\infty}^{\infty} e^{-imk_L x} A_m(s) + \frac{1}{k_L} \sum_{m=-\infty}^{\infty} e^{-imk_L x} \\ \times \int_{-\pi/L}^{\pi/L} A_m(s') F_e[x, s-s', \sigma\beta_m(p+s')] ds' \\ = F_e[x, s, \sigma\beta_0(p)] - F_e[x, s, -\sigma\beta_0(p)]. \end{aligned} \quad (22)$$

It should be noted that (22) involves only periodic functions of  $x$  with the period  $L$ . This is because any function of  $x$  is transformed into a periodic function

of  $x$  by the periodic Fourier transformation. Here,  $F_e[x, s, \sigma\beta_m(p)]$  is the periodic Fourier transform of  $f_e[x, \sigma\beta_m(p)]$ ,

$$f_e[x, \sigma\beta_m(p)] \iff F_e[x, s, \sigma\beta_m(p)], \quad (23)$$

where the symbol  $\iff$  denotes the relation between the periodic Fourier transform and its inverse, as is described in Appendix. Since  $F_e[x, s, \sigma\beta_m(p)]$  is a periodic function of  $x$  by (A.2), we write

$$F_e[x, s, \sigma\beta_n(p)] = \sum_{m=-\infty}^{\infty} C_m[s, \sigma\beta_n(p)] e^{-imk_L x}. \quad (24)$$

Form (24) and (22), one easily finds an integral equation for the amplitude  $A_m(s)$  as

$$\begin{aligned} A_m(s) + \frac{1}{k_L} \sum_{l=-\infty}^{\infty} \int_{-\pi/L}^{\pi/L} C_{m-l}[s-s', \sigma\beta_l(p+s')] \\ \times A_l(s') ds' = C_m[s, \sigma\beta_0(p)] - C_m[s, -\sigma\beta_0(p)]. \end{aligned} \quad (25)$$

It is still open question to find out an efficient method for solving (25). In the next section, however, we give an analytical solution by the small perturbation method.

### 4. Perturbation

Assuming  $\sigma k \ll 1$  and the corrugation height is sufficiently small, we solve the integral Eq. (25) by the small perturbation method.

We first expand  $C_m[s, \sigma\beta_l(p)]$  and  $A_m(s)$  into power series of the small parameter  $\sigma$ ,

$$\begin{aligned} C_m[s, \sigma\beta_l(p)] = \sigma C_m^{(1)}[s, \beta_l(p)] \\ + \sigma^2 C_m^{(2)}[s, \sigma\beta_l(p)] + \dots, \end{aligned} \quad (26)$$

$$A_m(s) = \sigma A_m^{(1)}(s) + \sigma^2 A_m^{(2)}(s) + \dots, \quad (27)$$

where  $A_m^{(1)}$  and  $A_m^{(2)}$  are the single and double scattering amplitudes, respectively. To calculate the coefficient  $C_m^{(n)}[s, \beta_l(p)]$ , we write

$$\begin{aligned} f_e[x, \sigma\beta_l(p+s')] \\ = i\sigma\beta_l(p+s')g(x|W) \sin(k_L x) \\ - \frac{1}{2}\sigma^2\beta_l^2(p+s')g^2(x|W) \sin^2(k_L x) + \dots \end{aligned} \quad (28)$$

Using (A.4), (A.6) and (A.8), we obtain

$$\begin{aligned} F_e(x, s, \sigma\beta_l(p+s')) = \frac{i\sigma}{L} \beta_l(p+s') \sin(k_L x) \\ \times \sum_{m=-\infty}^{\infty} e^{-imk_L x} G_1(s + mk_L|W) - \frac{\sigma^2}{2L} \beta_l^2(p+s') \\ \times \sin^2(k_L x) \sum_{m=-\infty}^{\infty} e^{-imk_L x} G_2(s + mk_L|W) + \dots, \end{aligned} \quad (29)$$

where  $G_n(s|W)$  is the Fourier spectrum of  $g^n(x|W)$ . From (24) and (29), we find

$$C_m^{(1)}[s, \beta_l(p)] = \frac{\beta_l(p)}{2L} [G_1(s + (m + 1)k_L|W) - G_1(s + (m - 1)k_L|W)]. \quad (30)$$

From (30), (27), (26) and (25), we obtain the single scattering amplitude,

$$A_m^{(1)}(s) = \frac{\beta_0(p)}{L} [G_1(s + (m + 1)k_L|W) - G_1(s + (m - 1)k_L|W)]. \quad (31)$$

Using (31), (30), (26) and (25), we obtain the double scattering amplitude,

$$A_m^{(2)}(s) = -\frac{\beta_0(p)}{4\pi L} \sum_{l=-\infty}^{\infty} \int_{-k_L/2}^{k_L/2} \beta_l(p + s') [G_1(s - s' + (m - l + 1)k_L|W) - G_1(s - s' + (m - l - 1)k_L|W)] \times [G_1(s' + (l + 1)k_L|W) - G_1(s' + (l - 1)k_L|W)] ds'. \quad (32)$$

By use of (31) and (32), we will calculate the scattering cross section later. However, we obtain approximate expressions for  $A_m^{(1)}(s)$  and  $A_m^{(2)}(s)$  to see effects of apodisation. When the width  $W$  is much larger than the wavelength  $\lambda$ ,  $|G_n(s|W)|$  becomes large at  $s = 0$ , as is shown in Fig. 2, but  $|G_n(s + mk_L|W)|$  is small when  $m \neq 0$ . Using such a localized property of  $G_n(s|W)$ , we obtain from (31) a rough approximation for  $A_m^{(1)}(s)$ ,

$$A_m^{(1)}(s) \approx 0, \quad m \neq \pm 1,$$

$$A_1^{(1)}(s) \approx -\frac{\beta_0(p)}{L} G_1(s|W),$$

$$A_{-1}^{(1)}(s) \approx \frac{\beta_0(p)}{L} G_1(s|W). \quad (33)$$

Also we obtain from (32) and (12) a rough approximation for  $A_m^{(2)}(s)$ ,

$$A_0^{(2)}(s) \approx \frac{\beta_0(p)}{2L} [\beta_1(p) + \beta_{-1}(p)] G_2(s|W),$$

$$A_2^{(2)}(s) \approx -\frac{\beta_0(p)}{2L} \beta_1(p) G_2(s|W),$$

$$A_{-2}^{(2)}(s) \approx -\frac{\beta_0(p)}{2L} \beta_{-1}(p) G_2(s|W),$$

$$A_m^{(2)}(s) \approx 0, \quad m \neq 0, \pm 2. \quad (34)$$

where we have used the relation:

$$G_2(s|W) = \frac{1}{2\pi} \int_{-\infty}^{\infty} G_1(s - s'|W) G_1(s'|W) ds'. \quad (35)$$

From (33) and (34), this paper obtains important conclusions such that the single scattering amplitude and the double scattering amplitude are proportional to  $G_1(s|W)$  and  $G_2(s|W)$ , respectively. Since  $|G_n(s|W)|^2$  becomes maximum at  $s = 0$ , the single scattering beams appear at  $\theta_s = \theta_{\pm 1}$  and the double scattering ones at  $\theta_s = \theta_0, \theta_{\pm 2}$ , where  $\theta_m$  is defined by (11). The intensity patterns of beams are proportional to  $|G_1(s|W)|^2$  and  $|G_2(s|W)|^2$  in single scattering and double scattering cases, respectively. Also, the beam intensities are proportional to  $|W_1|^2 = |G_1(0|W)|^2$  and  $|W_2|^2 = |G_2(0|W)|^2$  in single scattering and double scattering cases, respectively. We note that the beam pattern generated by the single scattering may differ from that by the double scattering. Since  $G_n(s|W)$  is a functional of  $g(x|W)$ , we may control the beam patterns by designing the apodisation function  $g(x|W)$ .

From (15) and (10), the beam width  $\Delta\theta_m^{(n)}$  for the  $m$ th diffraction order generated by the  $n$ -tuple scattering is given as

$$\Delta\theta_m^{(n)} = \frac{1}{k \sin \theta_m} \Delta S^{(n)}, \quad (36)$$

which well approximates the half-power beam angle for  $W_1 \gg \lambda$ .

### 5. Examples

Using the single and double scattering amplitudes, we calculate the scattering cross section for several apodisation functions. We consider the rectangular weight, Hanning and Hamming windows as examples of apodisation. For numerical calculations in what follows, we set

$$\theta_i = \frac{\pi}{3}, \quad L = 2.5\lambda, \quad W_1 = 50\lambda, \quad \sigma = 0.1\lambda. \quad (37)$$

#### 5.1 Apodisation Functions

Let us consider the apodisation function

$$g(x|W) = \begin{cases} a_1 + a_2 \cos\left(\frac{2\pi x}{W}\right), & |x| \leq W/2 \\ 0, & |x| > W/2 \end{cases}, \quad (38)$$

$$a_1 + a_2 = 1. \quad (39)$$

From (38), (13) and (15), the width parameters and the spectrum width  $\Delta S^{(n)}$  become

$$W_1 = a_1 W, \quad W_2 = \left(a_1^2 + \frac{a_2^2}{2}\right) W, \quad (40)$$

$$\Delta S^{(1)} = \frac{2\pi}{W} \left(1 + \frac{a_2^2}{2a_1^2}\right), \quad (41)$$

$$\Delta S^{(2)} = \frac{2\pi}{W} \frac{a_1^4 + 3a_1^2 a_2^2 + \frac{3}{8} a_2^4}{\left(a_1^2 + \frac{a_2^2}{2}\right)^2}. \quad (42)$$

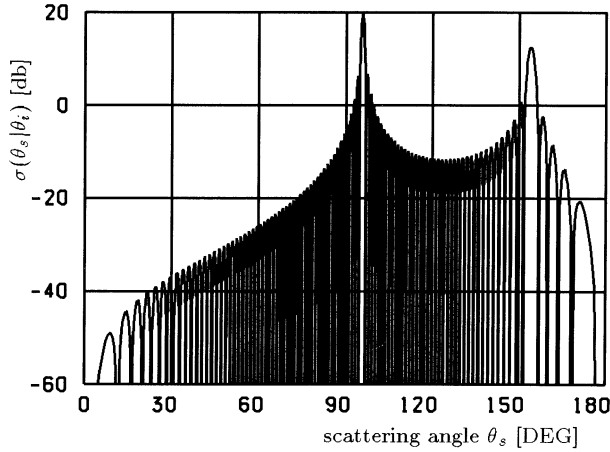


**Fig. 3** Scattering cross section  $\sigma(\theta_s|\theta_i)$  calculated only by single scattering amplitude. Rectangular weight.  $L = 2.5\lambda$ ,  $W_1 = W = 20L = 50\lambda$ ,  $\sigma = 0.1\lambda$  and  $\theta_i = \pi/3$ ,  $\lambda$  being the wavelength. The single scattering appears as the diffraction peaks at  $\theta_{-1} = 95.7^\circ$  and  $\theta_1 = 154.2^\circ$ . In case of the rectangular weight, sidelobes are high in level and spread widely.

## 5.2 Rectangular Weight

When

$$a_1 = 1, \quad a_2 = 0, \quad (43)$$

$g(x|W)$  becomes the rectangular function:

$$g(x|W) = u(x|W) \quad (44)$$

Here, the width  $W$  must be  $W = nL$  to make  $f(x)$  be continuous at  $x = \pm W/2$ , where  $n$  is any positive integer. By (12) and (44), one easily finds

$$G_1(s|W) = G_2(s|W) = W \frac{\sin\left(\frac{sW}{2}\right)}{\left(\frac{sW}{2}\right)}, \quad (45)$$

$$W_1 = W_2 = G_1(0|W) = G_2(0|W) = W, \quad (46)$$

$$\Delta S^{(1)} = \Delta S^{(2)} = \frac{2\pi}{W}. \quad (47)$$

Only in case of the rectangular weight,  $W_1$  and  $W_2$  are equal to the physical width  $W$ .

Figure 3 shows the scattering cross section computed by only the single scattering amplitude (31). The mainlobes appear at scattering angles  $\theta_1 = 154.2^\circ$  and  $\theta_{-1} = 95.7^\circ$ , where  $\theta_{-1}$  and  $\theta_1$  are the  $-1$ st and  $1$ st order diffraction angles given by (11). Since the single scattering amplitude  $A_m^{(1)}(s)$  is given by  $G_1(s|W)$  with the form  $\sin(x)/x$ , sidelobes appear around a beam peak in the angular distribution. The highest sidelobe associated with a mainlobe is only  $-13$  dB lower than its mainlobe peak.

Figure 4 shows the scattering cross section using the single scattering amplitude (31) and the double

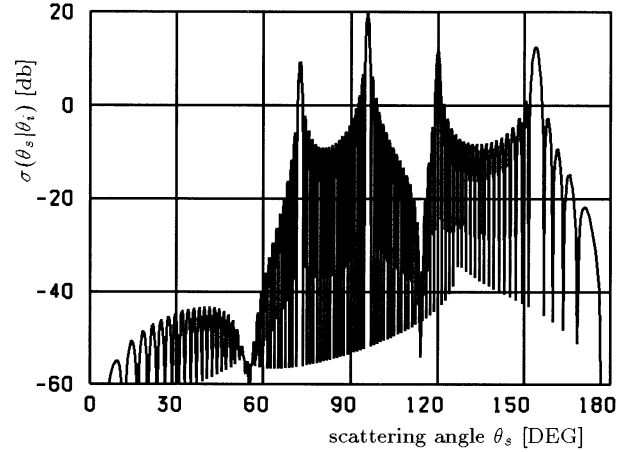


**Fig. 4** Scattering cross section  $\sigma(\theta_s|\theta_i)$  calculated by single and double scattering amplitudes. Rectangular weight. In addition to the single scattering peaks in Fig.3, double scattering appears as the diffraction peaks at  $\theta_{-2} = 72.5^\circ$  and  $\theta_0 = 120.0^\circ$ . Due to destructive interference between sidelobes generated by single and double scatterings, sidelobes are much reduced for  $\theta_s < 60^\circ$ .

scattering amplitude (32). In addition to the single scattering peaks, we see double scattering peaks at  $\theta_{-2} = 72.5^\circ$  and  $\theta_0 = 120.00^\circ$ , which correspond to the  $-2$ nd and  $0$  diffraction orders, respectively. However, the  $2$ nd order diffraction becomes invisible in case of (37). We note that the third order perturbation gives an additional peak at  $\theta_s = \theta_{-3} = 45.57^\circ$ , which does not appear in our approximation up to the second order perturbation. Sidelobes associated with the single and double scattering peaks may interfere each other. We see in Fig. 4 a destructive interference takes place for  $\theta_s < 60^\circ$ . From (47), and (37), the beam width is calculated as  $\Delta\theta_{-1}^{(1)} = 1.2^\circ$ ,  $\Delta\theta_1^{(1)} = 2.6^\circ$ ,  $\Delta\theta_{-2}^{(2)} = 1.2^\circ$  and  $\Delta\theta_0^{(2)} = 1.3^\circ$ .

We have seen that the rectangular weight generates a lot of sidelobes in the angular distribution of the scattering. These sidelobe levels may be much reduced, if one employs an appropriate weight instead of the rectangular weight. Such a weight is known as windows [9] in the harmonic analysis, current distributions in the antenna theory [10] and apodisation in optics [11].

## 5.3 Hanning Window

If we put

$$a_1 = a_2 = 0.5, \quad (48)$$

(38) becomes the Hanning Window. The scattering cross section using the single scattering amplitude (31) and the double scattering amplitude (32) is illustrated in Fig. 5, where we put  $W = 100\lambda$  to make  $W_1 = 50\lambda$  by (40). We see the single scattering beams at  $\theta_1 = 154.2^\circ$  and  $\theta_{-1} = 95.7^\circ$  and the double scattering peaks at  $\theta_{-2} = 72.5^\circ$  and  $\theta_0 = 120.00^\circ$ .

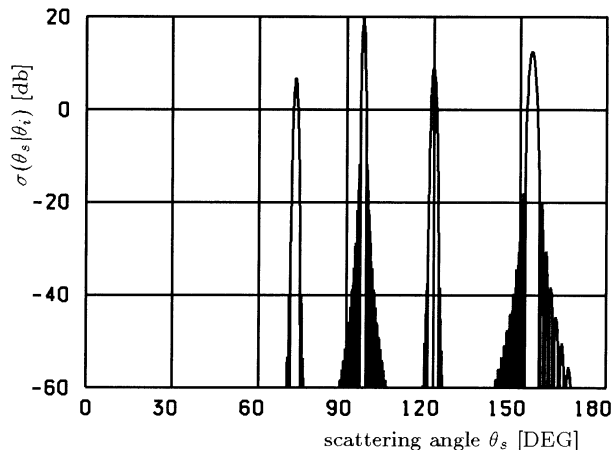


**Fig. 5** Scattering cross section  $\sigma(\theta_s|\theta_i)$  calculated by single and double scattering amplitudes. Hanning window.  $W_1 = 50\lambda$ ,  $W = 40L = 100\lambda$ . Peaks at  $\theta_{-1} = 95.7^\circ$  and  $\theta_1 = 154.2^\circ$  are the single scattering beams, of which sidelobes are much reduced in level and fall off quickly. The double scattering appears at  $\theta_{-2} = 72.5^\circ$  and  $\theta_0 = 120.00^\circ$ . Sidelobe distributions of a double scattering beam are different from those of a single scattering beam.

In case of the Hanning window, the sidelobes are much reduced. The highest sidelobe associated with a single scattering peak becomes  $-32$  dB down from the peak. In case of a double scattering peak, however, the highest sidelobe level becomes  $-46$  dB lower than its peak level. We pointed out above that the single scattering beam and the double scattering beam may have different patterns of angular distributions. This fact is clearly seen in Fig. 5, where sidelobe patterns are entirely different in the single scattering and double scattering cases. The sidelobes associated with the double scattering fall off much faster than those with the single scattering. However, such difference does not appear in case of the rectangular weight with  $|G_1(s|W)|^2 = |G_2(s|W)|^2$ . In case of the Hanning window, the beam width becomes slightly narrower than the rectangular case, because the corrugation width  $W = 100\lambda$  is much wider than  $W = 50\lambda$  in the rectangular case. From (48), (41), (42), and (37), the beam width may be calculated as  $\Delta\theta_{-1}^{(1)} = 0.9^\circ$ ,  $\Delta\theta_1^{(1)} = 2.0^\circ$ ,  $\Delta\theta_{-2}^{(2)} = 1.2^\circ$  and  $\Delta\theta_0^{(2)} = 1.3^\circ$ .

#### 5.4 Hamming Window

On the other hand, (38) becomes the Hamming Window [6] when

$$a_1 = \frac{1.08}{2}, \quad a_2 = \frac{0.92}{2}, \quad (49)$$

which are slightly different in numerical values from (48). However, the angular distribution of  $\sigma(\theta_s|\theta_i)$  becomes quite different as is illustrated in Fig. 6, where we put  $W = 92.59\lambda$  to make  $W_1 = 50\lambda$  by (40). Again, the single scattering peaks appear at  $\theta_1 = 154.2^\circ$

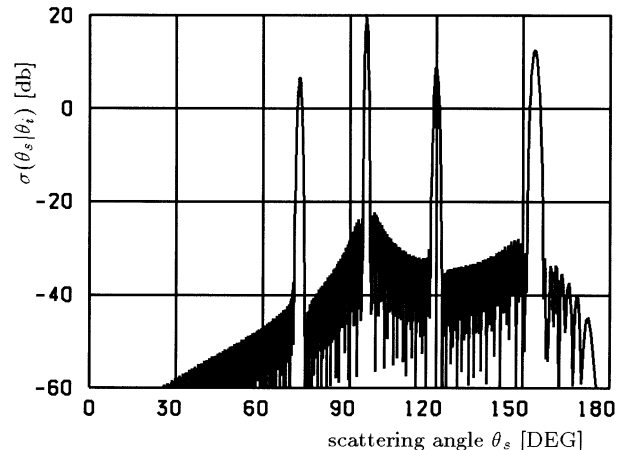


**Fig. 6** Scattering cross section  $\sigma(\theta_s|\theta_i)$  calculated by single and double scattering amplitudes. Hamming window.  $W_1 = 50\lambda$ ,  $W = 92.59\lambda$ . Peaks at  $\theta_{-1} = 95.7^\circ$  and  $\theta_1 = 154.2^\circ$  are the single scattering beams, of which sidelobes are much reduced. The double scattering appears at  $\theta_{-2} = 72.5^\circ$  and  $\theta_0 = 120.00^\circ$ .

and  $\theta_{-1} = 95.7^\circ$  and the double scattering peaks at  $\theta_{-2} = 72.5^\circ$  and  $\theta_0 = 120.00^\circ$ . The highest sidelobe associated with a single scattering peak becomes  $-43$  dB lower than its peak. In case of a double scattering peak, however, the highest sidelobe level is  $-49$  dB down from its peak value. Comparing Fig. 6 with Figs. 4 and 5 we see that sidelobe levels are relatively low in case of the Hamming window but the sidelobes fall off slowly, compared with the Hanning case. The beam width becomes  $\Delta\theta_{-1}^{(1)} = 0.8^\circ$ ,  $\Delta\theta_1^{(1)} = 1.9^\circ$ ,  $\Delta\theta_{-2}^{(2)} = 1.2^\circ$  and  $\Delta\theta_0^{(2)} = 1.3^\circ$ .

## 6. Conclusions

We have studied the wave scattering by an apodised sinusoidal surface. By use of the method of periodic Fourier transform and the small perturbation method, we obtain the single and double scattering amplitudes. Then, it is found that the beam shape generated by the single scattering is proportional to the Fourier spectrum of the apodisation function but that generated by the double scattering is proportional to the spectrum of the squared value of apodisation. Thus, the beam shape by the single scattering is different from that by the double scattering. We have demonstrated that the sidelobes are much reduced in level and in angular distribution by use of an apodisation function such as the Hanning window and Hamming window. This fact may be useful for designing devices using finite periodic structures such as diffraction gratings, leaky wave antenna and waveguide couplers.

However, our discussions are limited to a case where a TE plane wave is incident and the surface corrugation is sufficiently small in height. However, we note that our formulation can be immediately applied to TM wave case and the wave scattering from a dielec-

tric wave guide with an apodised periodic corrugation. It is still open question to find out an efficient method solving the integral Eq. (25) for a very rough case. It seems interesting to determine  $A_m(s)$  in the extended Floquet form by the Yasuura mode-matching method [12]. However, these problems are left for future study.

## References

- [1] W.S. Park and S.R. Seshadri, "Reradiation from a grating coupler for a grounded dielectric slab waveguide," IEE Proc. H, vol.133, no.1, pp.10–17, 1986.
- [2] M. Tomita, "Thin-film waveguide with a periodic groove structure of finite extent," J. Opt. Soc. Am. A., vol.6, no.9, pp.1455–1469, 1989.
- [3] K. Kobayashi and T. Eizawa, "Plane wave diffraction by a finite sinusoidal grating," IEICE Trans., vol.E74, no.9, pp.2815–2826, Sept. 1991.
- [4] R.A. Depine and D.C. Skigin, "Scattering from metallic surface having a finite number of rectangular grooves," J. Opt. Soc. Am., vol.A11, no.11, pp.2844–2850, 1994.
- [5] M. Nishimoto and H. Ikuno, "Space-wavenumber analysis of near fields around a finite periodic structure," Technical Report, EMT-97-20, pp.19–23, IEE Japan, 1997.
- [6] M. Tomita, "Analysis for scattering problem of directional coupler for slab waveguide," IEICE Trans. Electron., vol.E80-C, no.11, pp.1482–1490, Nov. 1997.
- [7] R. Petit, ed., Electromagnetic theory of gratings, Springer, Berlin, 1980.
- [8] J. Nakayama, "Periodic Fourier transform and its application to wave scattering from a finite periodic surface," IEICE Trans. Electron., vol.E83-C, no.3, pp.481–487, March 2000.
- [9] F.J. Harris, "On the use of windows for harmonic analysis with the discrete Fourier transform," Proc. IEEE, vol.66, no.1, pp.51–83, 1978.
- [10] T.T. Taylar, "Design of line-source antennas for narrow beamwidth and low side lobes," IRE Trans. Antennas & Propag., vol.AP-3, no.1, pp.16–28, 1955.
- [11] B. Malo, S. Theriault, D.C. Johnson, F. Bilodeau, J. Albert, and K.O. Hill, "Apodised in-fiber Bragg grating reflectors photoimprinted using a phase mask," Electron. Lett., vol.31, no.3, pp.223–225, 1995.
- [12] K. Yasuura, K. Shimohara, and T. Miyamoto, "Numerical analysis of a thin-film waveguide by mode-matching method," J. Opt. Soc. Am., vol.70, no.2, pp.183–191, 1980.

## Appendix: Periodic Fourier Transformation

This appendix summarizes properties of the periodic Fourier transform. See reference [8] for details.

We define the periodic Fourier transform of a function  $f(x)$  by

$$F(x, s) = e^{isx} \sum_{m=-\infty}^{\infty} e^{ismL} f(x + mL), \quad (\text{A} \cdot 1)$$

where the spectrum  $F(x, s)$  becomes a periodic function of  $x$  with the period  $L$ ,

$$F(x + mL, s) = F(x, s). \quad (\text{A} \cdot 2)$$

From (A.1), we formally find the inverse transform as

$$f(x) = \frac{1}{k_L} \int_{-\pi/L}^{\pi/L} F(x, s) e^{-isx} ds, \quad k_L = \frac{2\pi}{L}. \quad (\text{A} \cdot 3)$$

For simplicity, we will denote the relation between the periodic Fourier transform and its inverse by the symbol:  $f(x) \iff F(x, s)$ .

**modulation** If  $f(x) \iff F(x, s)$ , then

$$f(x) e^{iqx} \iff F(x, s + q). \quad (\text{A} \cdot 4)$$

**product of weighting function and periodic function** Let  $w(x)$  and  $f_p(x)$  be a weighting function and a periodic function with  $f_p(x) = f_p(x + L)$ , respectively. If we write

$$w(x) \iff F_w(x, s), \quad (\text{A} \cdot 5)$$

then, a product  $f_p(x)w(x)$  is transformed into a product of the periodic function and the periodic Fourier transform of the weighting function

$$f_p(x)w(x) \iff f_p(x)F_w(x, s), \quad (\text{A} \cdot 6)$$

which means that a periodic factor is invariant under the periodic Fourier transform. This is an important property of the periodic Fourier transform.

**relation with Fourier spectrum** Let  $\hat{F}(s)$  be the Fourier spectrum of  $f(x)$ ,

$$f(x) = \frac{1}{2\pi} \int_{-\infty}^{\infty} e^{-isx} \hat{F}(s) ds. \quad (\text{A} \cdot 7)$$

The spectrum  $F(x, s)$  is related with  $\hat{F}(s)$  as

$$F(x, s) = \frac{1}{L} \sum_{m=-\infty}^{\infty} e^{-imk_L x} \hat{F}(s + mk_L). \quad (\text{A} \cdot 8)$$



**Junichi Nakayama** received the B.E. degree from Kyoto Institute of Technology in 1968, M.E. and Dr. Eng. degrees from Kyoto University in 1971 and 1982, respectively. From 1971 to 1975 he worked in the Radio Communication Division of Research Laboratories, Oki Electric Industry, Tokyo. In 1975, he joined the staff of Faculty of Engineering and Design, Kyoto Institute of Technology, where he is currently Professor of Electronics and Information Science. From 1983 to 1984 he was a Visiting Research Associate in Department of Electrical Engineering, University of Toronto, Canada. His research interests are electromagnetic wave theory, acoustical imaging and signal processing. Dr. Nakayama is a member of IEEE and American Geophysical Union.